

Density-matrix renormalization group algorithm for non-Hermitian systems

Peigeng Zhong,¹ Wei Pan,¹ Haiqing Lin,^{1,2,*} Xiaoqun Wang,^{2,†} and Shijie Hu^{1,3,‡}

¹*Beijing Computational Science Research Center, Beijing 100084, China*

²*School of Physics, Zhejiang University, Hangzhou, 310058, China*

³*Department of Physics, Beijing Normal University, Beijing, 100875, China*

A biorthonormal-block density-matrix renormalization group algorithm is proposed to compute properties of non-Hermitian many-body systems, in which a structured low-rank approximation to a non-Hermitian reduced density matrix is implemented to fulfill the prerequisite for the biorthonormality of the renormalization transformation and to optimally construct a saved space as well. A redundancy assigned to the saved space of the reduced density matrix is exploited to reduce a condition number resulting from the left and right transformation matrices, thus ensuring the numerical stability of the renormalization procedure. The algorithm is successfully applied to an interacting fermionic Su-Schrieffer-Heeger model with both nonreciprocal hoppings and staggered complex chemical potential, exhibiting novel many-body phenomena in the ground-state phase diagram.

Non-Hermitian quantum systems in recent years have become of great interest in the exploration of the intriguing biorthogonal physics associated with nontrivial topology [1], exceptional points (EPs) [2], and non-Hermitian skin effects [3]. These phenomena are expected to be observable in photonic quantum walks [4], ultracold atomic gases [5], and other interdisciplinary studies [6–8]. More recently, non-Hermitian many-body effects have been increasingly addressed for spin liquids [9], topological states [10–16], and fractional quantum Hall states [17]. However, most efforts so far have mainly been cast into a few integrable models [18, 19] and special limits [20], demanding more efficient numerical tools.

Density-matrix renormalization group (DMRG) has achieved great success in studies of low-energy properties of a number of (quasi-)one-dimensional (1D) interacting systems [23, 24] and in extension to two-dimensional cases, but it does not yet seem to be available for non-Hermitian Hamiltonian systems [10, 20]. A non-Hermitian Hamiltonian H maps a right eigenstate to the corresponding left one, as sketched in Fig. 1(a), which gives rise to a non-Hermitian reduced density matrix ρ . Consequently, a DMRG procedure is defined to construct successively both the left Hilbert space $\tilde{\mathcal{H}}$ and the right one \mathcal{H} , as depicted in Fig. 1(b), in terms of the truncated left and right spaces of ρ , which form two transformation matrices simultaneously to renormalize the Hamiltonian $H_{g_n}^{\triangleleft}$ for the left semi-chain (\triangleleft) in the n -th step of the infinite-chain algorithm [23, 24]. The procedure ends when the computed quantities converge, corresponding to the infinite-block-size limit of $g_n = \infty$. In a Hermitian case, $\mathcal{H} \equiv \tilde{\mathcal{H}}$, and there exists a unitary operator U_n (written as a matrix hereafter) and an operation \mathcal{U}_n such that a renormalization group (RG) transformation $H_{g_{n+1}}^{\triangleleft} = \mathcal{U}_n[H_{g_n}^{\triangleleft}] = U_n^\dagger H_{g_n}^{\triangleleft} U_n$ can be carried out between two successive block sizes of g_{n+1} and g_n . The bare counterpart $H_{g_1 \equiv 1}^{\triangleleft} \equiv H^{\triangleleft}$ is thus directed towards a fixed point $H_\infty^{\triangleleft} = \mathcal{U}_\infty[\dots \mathcal{U}_1[H^{\triangleleft}]]$ following an RG trajectory [25]. On the contrary, in a non-Hermitian system where $\mathcal{H} \neq \tilde{\mathcal{H}}$ for $n > 1$, a similarity transfor-

mation of $\mathcal{Y}_n[H_{g_n}^{\triangleleft}] = \bar{Y}_n H_{g_n}^{\triangleleft} Y_n$ has to be constructed to preserve its spectrum, and $\bar{Y}_n \neq Y_n^{-1}$ when truncation is made. As a result, a fixed point is reached with $H_\infty^{\triangleleft} = \mathcal{Y}_\infty[\dots \mathcal{Y}_1[H^{\triangleleft}]]$. This feature can be demonstrated in a pseudo-Hermitian case, where an invertible matrix η is used to find an equivalent Hermitian Hamiltonian $H^{\triangleleft(h)}$ via the transformation $H^{\triangleleft(h)} = \eta H^{\triangleleft} \eta^{-1}$ [26]. Subsequently, a unitary matrix $U_n = \eta Y_n \eta^{-1}$ can be found to ensure that the fixed point of H^{\triangleleft} aligns with that of $H^{\triangleleft(h)}$ using standard DMRG iterations. However, more general non-Hermitian systems, which may involve intricate many-body interactions proposed in recent theoretical studies, inevitably pose severe challenges [20].

Inspiringly, the transfer-matrix renormalization group (TMRG) method has been successfully developed to handle a peculiar non-Hermitian matrix, presented in a special form of a transfer-matrix product that is tailored for computing thermodynamic properties in (quasi-)1D [24]. Since then, more efforts have been devoted to solving problems related to non-Hermitian Hamiltonians, which simulate dynamical phase transitions [27], electron motion in artificial fluxes [28], reaction-diffusion equations [29], and quantum stochastic processes [30–32]. These studies strikingly call for the exploration of a general non-Hermitian DMRG algorithm to confront both the complex similarity transformation and numerical stability, essentially to ensure the reliability of calculations.

In this letter, we develop a biorthonormal-block DMRG (bbDMRG) algorithm that tackles the challenges encountered in the practical implementation of similarity transformations, which are constructed in terms of the optimally selected bases. Our algorithm introduces a structured low-rank approximation of the non-Hermitian reduced density matrix, takes advantage of redundant degrees of freedom to mitigate numerical instability, and employs an advanced two-sided Krylov-Schur-restarted Arnoldi (TS-KSRA) diagonalization technique [33]. It enables large-scale numerical simulations far beyond the capabilities of existing methods. Successful applications of our algorithm are shown to reveal non-

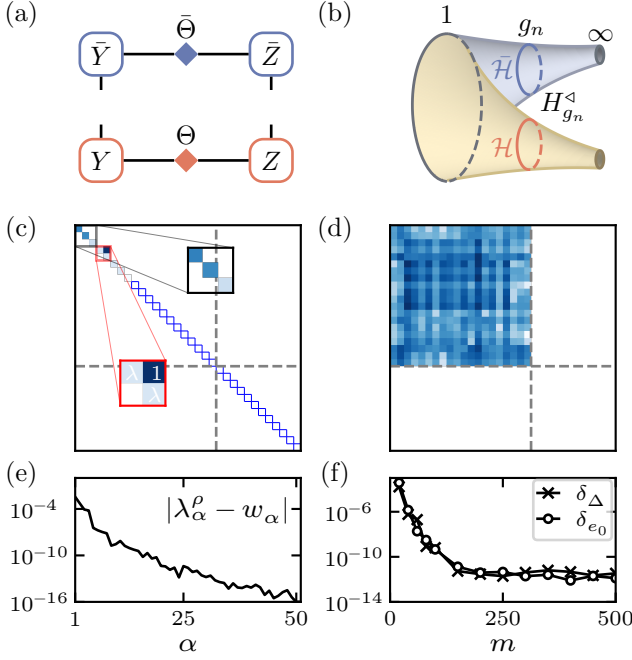


FIG. 1. (Color online) (a) A sketch of the decompositions of the biorthonormal left and right eigenstates of H with respect to two semi-chains. (b) A schematic RG display of dual spaces $\bar{\mathcal{H}}$ and \mathcal{H} corresponding to $H_{g_n}^{\triangleleft}$ of the left semi-chain. (c-f) Tests on the SSH model (4) under open boundary conditions. (c) and (d) Block-diagonal forms of ρ with $t_1 = 1.5$, $t_2 \approx 0.96$ [21], $\gamma = V = 2$, and a chain of $N = 4$ unit cells segmented into two subsets of 5 left and 3 right sites. (c) GEVD-based Jordan normal form [22] consisting of ordinary eigenvalues (■ in black box), rank-2 Jordan block (red box), and null spaces (□). (d) Two-block-diagonal form by a two-step technique (see text). (e) $|\lambda_\alpha^\rho - w_\alpha|$ between the singular value λ_α^ρ and weight w_α for $N = 50$, $m = 100$, $t_1 = 0.7$ and $V = 5$. (f) Absolute errors δ_{e_0} and δ_Δ for the exact ground-state energy e_0 and the gap $\Delta = e_1 - e_0$, respectively, versus the truncation dimension m for $N = 50$, $t_1 = 0.7$ and $V = 0$.

Hermitian many-body effects in the interacting fermionic Su–Schrieffer–Heeger (SSH) chain.

Biorthonormal-block representation. Two mutually dual spaces are necessarily used in the RG transformation over non-Hermitian Hamiltonians $H^{\triangleleft, \triangleright}$ [34] and other operators for either left (\triangleleft) or right (\triangleright) semi-chains. The left eigenstate $\langle \bar{\Psi} |$ and the right one $|\Psi\rangle$ holding $\langle \bar{\Psi} | \Psi \rangle = 1$, obey a pro forma variational principle $\min | \langle \bar{\Psi} | H | \Psi \rangle - e |$ with $H = H^{\triangleleft} + H^{\triangleleft \triangleright} + H^{\triangleright}$, where $H^{\triangleleft \triangleright}$ couples two semi-chains, the complex energy e is presumably predetermined, such that $\langle \bar{\Psi} | H = e \langle \bar{\Psi} |$ and $H | \Psi \rangle = e | \Psi \rangle$.

Analogous to DMRG for the Hermitian case, our bbDMRG algorithm looks for a fixed point of targeted-state wave functions, as illustrated in Fig. 1(a,b),

$$\langle \bar{\Psi} | = \sum_{\alpha, \alpha'} \langle \bar{y}_\alpha | \bar{\Theta}_{\alpha, \alpha'} \langle \bar{z}_{\alpha'} |, \quad | \Psi \rangle = \sum_{\alpha, \alpha'} | y_\alpha \rangle \Theta_{\alpha, \alpha'} | z_{\alpha'} \rangle. \quad (1)$$

Both are partitioned into \triangleleft and \triangleright parts with dimensions of d^\triangleleft and d^\triangleright , respectively, and the total dimension $d^T = d^\triangleleft d^\triangleright$. The basis sets $\langle \bar{y}_\alpha |$, $\langle \bar{z}_{\alpha'} |$, $| y_\alpha \rangle$ and $| z_{\alpha'} \rangle$ are linked to bare counterparts through similarity transformation matrices \bar{Y} , \bar{Z} , Y and Z , respectively [22], where $\langle \bar{y}_\alpha | y_{\alpha'} \rangle = \langle \bar{z}_\alpha | z_{\alpha'} \rangle = \delta_{\alpha, \alpha'}$ and $\bar{Y}Y = \bar{Z}Z = \mathbb{1}$. Matrices $\bar{\Theta}$ and Θ are nondiagonal, unlike the biorthonormal matrix product representation suited for Perron states [35].

To elucidate the bbDMRG algorithm, we focus on the left semi-chain with a non-Hermitian reduced density matrix $\rho = \text{tr}_{\triangleright} |\Psi\rangle \langle \bar{\Psi}|$. It is a key concept that the m most optimal pairs of $\langle \bar{y}_\alpha |$ and $| y_\alpha \rangle$ are presumably constructed into a saved (s) space $\bar{Y}^{(s)}$ and $Y^{(s)}$ for the RG transformation, while the rest is discarded (d) as $\bar{Y}^{(d)}$ and $Y^{(d)}$. It turns out that ρ may be written as a block diagonal

$$\rho = (Y^{(s)} \quad Y^{(d)}) \begin{pmatrix} B^{(s)} & \mathbb{0} \\ \mathbb{0} & B^{(d)} \end{pmatrix} \begin{pmatrix} \bar{Y}^{(s)} \\ \bar{Y}^{(d)} \end{pmatrix}, \quad (2)$$

which defines $\rho^{(s,d)} = Y^{(s,d)} B^{(s,d)} \bar{Y}^{(s,d)}$ with two block matrices $B^{(s,d)}$ such that $[\rho^{(s)}, \rho^{(d)}] = 0$. As seen in Figs. 1(c, d), $B^{(s,d)}$ can be either a dense matrix or composed of some subblocks in diagonal, including 1×1 matrix with an eigenvalue ζ_α or a nondiagonalizable Jordan block, and $\rho^{(s)}$ is a low-rank approximation to ρ [22].

Prior to constructing $B^{(s)}$, it is necessary to address a crucial issue of how optimal a saved space could be as revealed by the error $\varepsilon = |\text{tr}[(\rho - \rho^{(s)})O]| = |\text{tr}(\rho^{(d)}O)|$ for the left-right (LR) measurement $\langle O \rangle_{\text{lr}} = \langle \bar{\Psi} | O | \Psi \rangle$ of a physical quantity O [22, 23, 36]. Similar to DMRG, although it is impossible to directly estimate ε because O and ρ are coupled, its upper bound (UB) can be found [36]. In particular, von Neumann’s trace inequality [37] gives rise to $\varepsilon \leq \sum_\alpha \lambda_\alpha^{\rho^{(d)}} \lambda_\alpha^O \equiv \varepsilon_1$, where $\lambda_\alpha^{\rho^{(d)}}$ and λ_α^O correspond to the singular values of $\rho^{(d)}$ and O sorted in descending order. By introducing $a = \sum_\alpha \lambda_\alpha^O$, a larger UB is given as $\varepsilon \leq \varepsilon_1 \leq \varepsilon_2 = a \|\rho^{(d)}\|_2$ with $\|\rho^{(d)}\|_2$ being the 2-norm of $\rho^{(d)}$. According to the Eckart–Young–Mirsky theorem widely used in tensor algorithms [38], $\|\rho^{(d)}\|_2$ has a minimum value of λ_{m+1}^ρ , which is the $(m+1)$ -th largest singular value of ρ . Consequently, one formally obtains $\varepsilon_2 = a \lambda_{m+1}^\rho$ as the UB of ε , consistent with that for Hermitian cases. In practice, unfortunately, it is known to be an NP-hard problem to simultaneously minimize ε_2 as well as satisfy the non-unitary RG requirement for spanning $\bar{\mathcal{H}}$ and \mathcal{H} in order to achieve the best *structured* low-rank approximation [39].

The strict condition on ε_2 can be significantly relaxed in practical applications. To achieve this, we sort the eigenvalue spectra $\{\zeta_\alpha\}$ of ρ in descending order of the semi-positive weight $w_\alpha = |\zeta_\alpha|$. This allows for the introduction of a larger UB $\varepsilon_3 = a \kappa w_{m+1} \geq \varepsilon_2$ after utilizing Cauchy–Schwarz inequality [22], where $\kappa = \|\bar{Y}\|_2 \|Y\|_2$ is a condition number. It turns out that both κ and w_{m+1} are supposed to be minimized as much as possible in the implementation of $\bar{Y}^{(s)}$ and $Y^{(s)}$. Specifically, κ measures the deviation strength of the non-Hermitian ρ from

the best approximation of all possible Hermitian ones to some extent. For Hermitian cases, $\kappa = 1$ and $w_\alpha = \zeta_\alpha$, resulting in $\varepsilon_3 = \varepsilon_2$ as anticipated [23]. In non-Hermitian cases, the block diagonalization of ρ can be executed in a way that the minimum $w_{\min}^{(s)}$ for $B^{(s)}$ is larger than the maximum $w_{\max}^{(d)}$ for $B^{(d)}$ [22]. We note that the singular value and eigenvalue spectra of ρ have a consistent profile with $\lambda_{\min}^\rho \leq w_\alpha \leq \lambda_{\max}^\rho$ and $|\lambda_\alpha^\rho - w_\alpha| \leq \|T\|_2$, which decreases rapidly with α as shown in Fig. 1(e), and T denotes the strictly upper triangular matrix in the Schur decomposition of ρ [22]. Therefore, ε_3 effectively stands for the UB of the measurement error ε for bbDMRG.

In general, it is impossible to construct $\bar{Y}^{(s)}$, $Y^{(s)}$ and $B^{(s)}$ directly by full diagonalization of a non-Hermitian ρ . Moreover, one cannot know how large κ could be prior to the determination of \bar{Y} and Y . To confront this challenge, we find a two-step approach to achieve the block-diagonalization of ρ . First, we convert ρ into its upper triangular form consisting of an $m \times m$ matrix A , a $(d^\triangleleft - m) \times (d^\triangleleft - m)$ matrix C and an $m \times (d^\triangleleft - m)$ matrix D , by using a Schur decomposition

$$\rho = S \begin{pmatrix} A & D \\ 0 & C \end{pmatrix} S^\dagger, \quad (3)$$

with a unitary matrix $S = (S^{(s)} \ S^{(d)})$. The diagonal elements of A and C give rise to eigenvalues ζ_α . In this step, we also sort ζ_α in descending order of w_α and are allowed to separate the full space into the saved and discarded spaces. Secondly, using Roth's removal rule and the Bartels-Stewart algorithm [22], we generate a similarity transformation matrix X to convert the upper triangular matrix into a block-diagonal form (2) by solving the Sylvester equation $AX - XC = D$. Lastly, in terms of A , C , S and X , we have $\bar{Y}^{(s)} = S^{(s)\dagger} + XS^{(d)\dagger}$, $\bar{Y}^{(d)} = S^{(d)\dagger}$, $Y^{(s)} = S^{(s)}$, $Y^{(d)} = S^{(d)} - S^{(s)}X$, $B^{(s)} = A$, and $B^{(d)} = C$ [22].

It is remarkable that $\kappa > 1$ directly affects the feasibility of the renormalization procedure. The larger κ results in more severe numerical instability with bigger errors and larger ε_3 , which are obstacles to earlier DMRG exploration [10, 20]. Nevertheless, we found that there still exists some redundancy in constructing the saved space. When an invertible matrix η is applied to the saved space $\bar{Y}_\eta^{(s)} = \eta^{-1}\bar{Y}^{(s)}$ and $Y_\eta^{(s)} = Y^{(s)}\eta$, the block-diagonal form in Eq. (2) remains unchanged [22]. This allows us to construct an appropriate $\bar{Y}_\eta^{(s)}$ and $Y_\eta^{(s)}$ so as to effectively reduce κ and then ε_3 . It turns out that the block $B_\eta^{(s)} = \bar{Y}_\eta^{(s)}\rho Y_\eta^{(s)} = \eta^{-1}B^{(s)}\eta$ may become dense, while the conventional truncation error $\varepsilon_t \approx 1 - \sum_{\alpha=1}^m |\zeta_\alpha|$ only depends on the spectra $\{\zeta_\alpha\}$ and is free of the choice of η . In practice, η as an $m \times m$ matrix can be obtained with good quality by various skills over $\bar{Y}^{(s)}$ and $Y^{(s)}$, and the rescaling of $H^{\triangleleft, \triangleright}$ often substantially enhances the precision of the bbDMRG results [40, 41].

Efficiency of the algorithm. We now turn to an ap-

plication of bbDMRG to an interacting fermionic SSH model on a duplex lattice of N unit cells under the open boundary condition (OBC) as described by

$$H_{\text{ssh}} = \sum_{\ell=1}^N \left(t_L c_{\ell,a}^\dagger c_{\ell,b} + t_R c_{\ell,b}^\dagger c_{\ell,a} + V n_{\ell,a} n_{\ell,b} \right) + \sum_{\ell=1}^{N-1} \left[t_2 (c_{\ell,b}^\dagger c_{\ell+1,a} + \text{h.c.}) + V n_{\ell,b} n_{\ell+1,a} \right] + \sum_{\ell=1}^N \sqrt{2} e^{-i\pi/4} u \left(n_{\ell,a} - n_{\ell,b} \right), \quad (4)$$

where $c_{\ell,\sigma}^\dagger$, $c_{\ell,\sigma}$, and $n_{\ell,\sigma} = c_{\ell,\sigma}^\dagger c_{\ell,\sigma}$, with $\sigma = a$ or b , represent creation, annihilation, and particle-number operators for the fermion, respectively. Accordingly, the displacement of the site- (ℓ, σ) is given by $x = 2\ell - 1$ for sublattice- a , while $x = 2\ell$ for sublattice- b . The number operators for fermions in the left and right semi-chains are defined as $N_{\triangleleft, \triangleright}^f = \sum_{\ell \in \triangleleft, \triangleright} (n_{\ell,a} + n_{\ell,b})$. The hopping coefficients $t_{L,R} = t_1 \mp \gamma$ have a nonreciprocity $\gamma \geq 0$ and $t_1 > 0$ for odd bonds, and $t_2 = 1$ for even bonds set as the energy unit. $V \geq 0$ represents the repulsion strength between fermions at nearest-neighboring (NN) sites, while u gives the strength of the staggered complex chemical potential. Unless explicitly stated, the following discussions focus on the ground state, possessing the minimal real part of the energy, at *half-filling* with $\gamma = 0.1$.

Figure 1(c) displays a Jordan normal form of ρ obtained using a regular generalized eigenvalue decomposition (GEVD) with a parameter set in the \mathcal{PT} -broken region for $N = 4$ [22]. In this case, we kept twenty generalized eigenvectors to construct the similarity transformation matrices. One DMRG step leads to an absolute error of $\delta_{e_0} = 10^{-7}$ for the ground state energy e_0 regardless of $\varepsilon_t = 0$, while the corresponding condition number $\kappa \approx 10^7 \gg 1$. On the contrary, when the block-diagonal decomposition is implemented using the two-step approach with those techniques discussed above, κ is reduced to 1 with obtaining δ_{e_0} at machine precision and the block for the saved space becomes dense as shown in Fig. 1(d). The bbDMRG calculations are also performed for $N = 50$ with $t_1 = 0.7$ and $V = 5$ to compute e_0 and the gap $\Delta = e_1 - e_0$, where e_1 is the first excitation energy based on the ascending order of the real part of energy values. One can see that both δ_{e_0} and δ_Δ converge to their lower bounds with increasing the truncation dimension m , as seen in Fig. 1(f). More benchmarks are provided in the Supplemental Material [22]. Below are two kinds of kink behaviors discussed for non-Hermitian many-body effects with the model (4).

Skin effects of a kink at $u = 0$. Figure 2(a) presents the phase diagram for a \mathcal{PT} -unbroken region of $t_1 \geq \gamma$ [43]. While a topological insulator (TI), a dimerized phase (DM), and a normal EP of $t_1 = \gamma$ have been explored intensively for $V = 0$ [44], we found newly a non-Hermitian

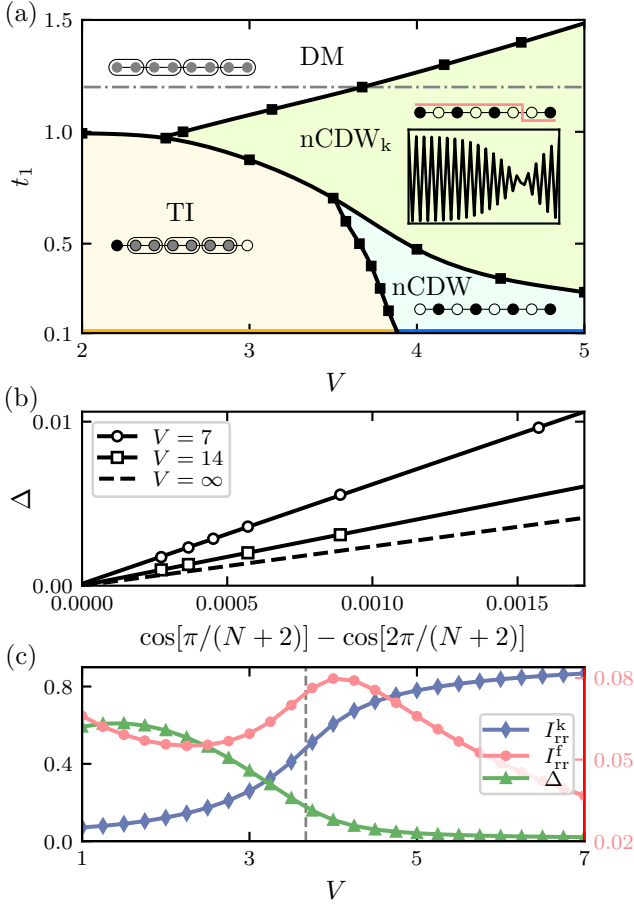


FIG. 2. (Color online) (a) The ground-state phase diagram: a topological insulator (TI, orange), a dimerized phase (DM, blank), a non-Hermitian charge density wave (nCDW, cyan), an nCDW with a kink (nCDW_k, green), a normal EP line (orange solid) and a CDW-EP line (blue solid). Black squares indicate transition points determined by peaks of the RR fidelity susceptibility [42] with $N = 48$. Inset: the density profile of fermions $\langle n_{\ell, \sigma} \rangle_{\text{rr}}$ at $t_1 = 0.7$, $V = 7$, and $N = 20$. (b) The imbalances: I_{rr}^k (◆) for the kink, I_{rr}^f (●) for the fermion, and smallest neutral gap Δ (△), as a function of the repulsion strength V for $N = 64$. The dashed line denotes the transition point $V_c \approx 3.6$ determined in (a). (c) Δ versus $\cos[\pi/(N+2)] - \cos[2\pi/(N+2)]$ with $N \in [96, 232]$, vanishing as $N \rightarrow \infty$. In (b) and (c), $t_1 = 1.2$ (dot-dashed line in (a)).

charge density wave (nCDW), an nCDW with a kink (nCDW_k), and a CDW-EP line, for sufficiently large V . The nCDW phase involves two-fold degenerate ground states in which the fermion density oscillates on two sublattices, resulting in two different configurations, nCDW-1: $(1_{1,a}, 0_{1,b}, \dots, 0_{N,b})$, and nCDW-2: $(0_{1,a}, \dots, 0_{N,a}, 1_{N,b})$ [22]. The CDW-EP line at $t_1 = \gamma$ arises from the exclusive principle of fermions on two nearest neighbor sites rather than skin effects at edges, occurring in the normal EP. This new effect cannot be simply explained in the context of the generalized Brillouin zone [45].

In the nCDW_k phase, a pair of holes emerge to form a kink, separating a left nCDW-1 from a right nCDW-2, as sketched in the inset of Fig. 2(a). The strong skin effect on the fermion density can be observed from a right-right (RR) measurement of $\langle n_{\ell} \rangle_{\text{rr}}$, associated with the position of the kink, as shown in Fig. 2(a). When $2V > (t_1^2 + t_2^2 - \gamma^2)/\sqrt{t_1^2 - \gamma^2}$, the kinetic energy of the kink adequately compensates for the chemical potential so that a kink is stably present in the ground state [22]. The motion of the kink yields a gap $\Delta = \chi[\cos(\pi/(N+2)) - \cos(2\pi/(N+2))]$ for the lowest excitation, as depicted in Fig. 2(b). As $V, N \rightarrow \infty$, χ gradually converges to $\chi_0 = 2\sqrt{t_1^2 - \gamma^2}$, in accordance with the predictions of the effective Hanot-Neldson model [22, 46]. When V is finite, $\chi > \chi_0$ reflects the contributions of the higher-order processes.

To interpret the nature of the nCDW_k phase, we also calculate the imbalance $I_{\text{rr}}^{\text{f,k}} = |\langle N_{\text{d}}^{\text{f,k}} - N_{\text{d}}^{\text{f,k}} \rangle_{\text{rr}}|$ for the fermion number $N_{\text{d}}^{\text{f,k}}$ as well as the kink number $N_{\text{d}}^{\text{k}} = \sum_{\ell \in \langle \text{d} \rangle} [(1 - n_{\ell,b})(1 - n_{\ell+1,a}) - n_{\ell,b}n_{\ell+1,a}]$. While I_{rr}^{f} quantifies the skin effect in the single-particle scenario, I_{rr}^{k} reveals many-body effects associated with the kink. Figure 2(c) displays I_{rr}^{f} and I_{rr}^{k} versus V along a dot-dashed line in Fig. 2(a), showing the transition between DM and nCDW_k phases at $t_1 = 1.2$. At $V = 0$, fermions are tightly bound within each local resonance bond in DM, resulting in a relatively weak skin effect. As V is switched on and increased, I_{rr}^{f} initially decreases and then increases again, but reaches its maximum just to the right of the DM-nCDW_k transition. As a many-body effect, I_{rr}^{k} increases monotonically from DM to nCDW_k with increasing V and is generally an order of magnitude larger than I_{rr}^{f} , making it easier to detect experimentally. In addition, we find that the excitation is gapped in the DM phase, but becomes gapless in the nCDW_k phase as seen in Figure 2(c).

Localization of a kink at $u \neq 0$. Figure 3 presents the results for the complex fermion density in (a-d) and the energy gap in (e, f). The skin effect of the kink for $u = 0$ is shown with $\langle n_{\ell, \sigma} \rangle_{\text{rr}}$ in Fig. 3(a). For a finite u , there is an effective chemical potential of $\mu_{\text{eff}} = u(1 - i)(2\ell - N)$ [22]. As u grows, the skin effect of the kink on the right side gradually weakens, leaving the kink localized on the left side of the chain, as seen in Figs. 3(b) and (c). It is noteworthy that the imaginary part $\text{Im} \langle n_{\ell, \sigma} \rangle_{\text{rr}}$ forms a localized wave packet for the kink, and the size of the wave packet is essentially governed by the staggered complex chemical potential, as illustrated in Fig. 3(d). Moreover, the gap remains finite in the thermodynamic limit (TDL) for non-zero u to characterize the localization of the kink, which can be found for both $\text{Re}\Delta$ and $\text{Im}\Delta$ as seen in Fig. 3(e) and (f), respectively.

Summary and discussion. A biorthonormal-block density-matrix renormalization group algorithm is presented to calculate complex properties of non-Hermitian

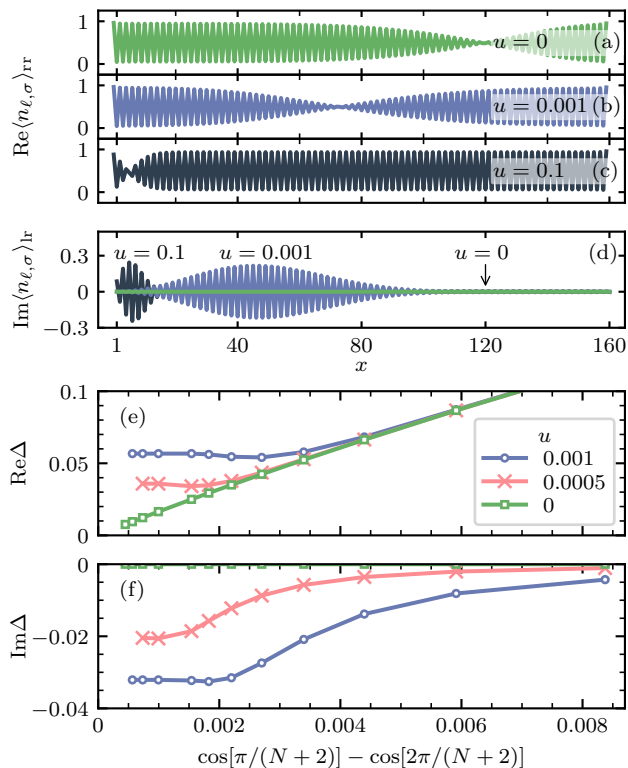


FIG. 3. (Color online) For $t_1 = 2$, $V = 10$, the real parts of $\langle n_{\ell,\sigma} \rangle_{\text{rr}}$ in (a)-(c) and imaginary parts of $\langle n_{\ell,\sigma} \rangle_{\text{lr}}$ in (d) for a chain with 80 unit cells, where the kink being sensitive to u migrates towards the left as the chemical potential u increases. (e)-(f): The real and imaginary parts of the energy gap Δ change with $N \leq 160$ and nonvanishing for $u > 0$.

many-body systems, such as the spectrum, the energy gap, and other relevant observables. Distinguishing from conventional techniques, a structured low-rank approach and the redundant degrees of freedom are implemented to construct the optimized saved space for the renormalization of operators from a non-Hermitian reduced density matrix. Numerical stability and efficiency are achieved by effectively reducing the condition number through the utilization of additional skills and rescaling techniques [40, 41]. Accurate calculations are shown for sizes that allow extrapolation to TDL, far beyond those of other recently developed methods [10, 47–49].

As applied to an interacting fermionic SSH model with nonreciprocal hoppings and staggered complex chemical potential, a ground-state phase diagram is established by finding the nCDW and nCDW_k phases, as well as a CDW-EP line. In particular, a new kind of skin effect emerges in connection to the dynamics of a kink, which gives rise to gapless excitation but becomes gapped in the presence of the chemical potential. The skin effect of the kink is an order of magnitude more pronounced than that of the fermion number, greatly enhancing the experimental visibility of non-Hermitian physics.

We are grateful to Tao Xiang, Ulrich Schollwöck, Ian Affleck, Walter Hofstetter, Zheng-Cheng Gu, Shi-Liang Zhu, and Shuo Yang for fruitful discussions. This work is supported by grants: MOST 2022YFA1402700, NSFC 12174020, NSFC 12088101, NSFC 11974244, and NSAF U1930402. Computational resources from Tianhe-2JK at the Beijing Computational Science Research Center and Quantum Many-body I cluster at SPA, Shanghai Jiao-tong University are also highly appreciated.

* haiqing0@csrc.ac.cn
† xiaoqunwang@zju.edu.cn
‡ shijiehu@csrc.ac.cn

- [1] Emil J. Bergholtz, Jan Carl Budich, and Flore K. Kunst, “Exceptional topology of non-Hermitian systems,” *Reviews of Modern Physics* **93**, 015005 (2021).
- [2] Ramy El-Ganainy, Konstantinos G. Makris, Mercedesh Khajavikhan, Ziad H. Musslimani, Stefan Rotter, and Demetrios N. Christodoulides, “Non-hermitian physics and PT symmetry,” *Nature Physics* **14**, 11 (2018).
- [3] Xiujuan Zhang, Tian Zhang, Ming-Hui Lu, and Yan-Feng Chen, “A review on non-Hermitian skin effect,” *Advances in Physics: X* **7**, 2109431 (2022).
- [4] Lei Xiao, Tianshu Deng, Kunkun Wang, Gaoyan Zhu, Zhong Wang, Wei Yi, and Peng Xue, “Non-hermitian bulk–boundary correspondence in quantum dynamics,” *Nature Physics* **16**, 761–766 (2020).
- [5] Wei Gou, Tao Chen, Dizhou Xie, Teng Xiao, Tian-Shu Deng, Bryce Gadway, Wei Yi, and Bo Yan, “Tunable nonreciprocal quantum transport through a dissipative aharonov-bohm ring in ultracold atoms,” *Physical Review Letters* **124**, 070402 (2020).
- [6] T. Gao, E. Estrecho, K. Y. Bliokh, T. C. H. Liew, M. D. Fraser, S. Brodbeck, M. Kamp, C. Schneider, S. Höfling, Y. Yamamoto, F. Nori, Y. S. Kivshar, A. G. Truscott, R. G. Dall, and E. A. Ostrovskaya, “Observation of non-hermitian degeneracies in a chaotic exciton-polariton billiard,” *Nature* **526**, 554–558 (2015).
- [7] Wengang Zhang, Xiaolong Ouyang, Xianzhi Huang, Xin Wang, Huili Zhang, Yefei Yu, Xiuying Chang, Yanqing Liu, Dong-Ling Deng, and L.-M. Duan, “Observation of non-hermitian topology with nonunitary dynamics of solid-state spins,” *Physical Review Letters* **127**, 090501 (2021).
- [8] Wei Wang, Xulong Wang, and Guancong Ma, “Non-hermitian morphing of topological modes,” *Nature* **608**, 50–55 (2022).
- [9] Kang Yang, Siddhardh C. Morampudi, and Emil J. Bergholtz, “Exceptional spin liquids from couplings to the environment,” *Physical Review Letters* **126**, 077201 (2021).
- [10] Dan-Wei Zhang, Yu-Lian Chen, Guo-Qing Zhang, Li-Jun Lang, Zhi Li, and Shi-Liang Zhu, “Skin superfluid, topological Mott insulators, and asymmetric dynamics in an interacting non-Hermitian Aubry-Andre-Harper model,” *Physical Review B* **101**, 235150 (2020).
- [11] Boran Zhou, Rui Wang, and Baigeng Wang, “Renormalization group approach to non-Hermitian topological quantum criticality,” *Physical Review B* **102**, 205116 (2020).

- (2020).
- [12] Tao Liu, James Jun He, Tsuneya Yoshida, Ze-Liang Xiang, and Franco Nori, “Non-Hermitian topological Mott insulators in one-dimensional fermionic superlattices,” *Physical Review B* **102**, 235151 (2020).
- [13] Ching Hua Lee, “Many-body topological and skin states without open boundaries,” *Physical Review B* **104**, 195102 (2021).
- [14] W. N. Faugno and Tomoki Ozawa, “Interaction-Induced Non-Hermitian Topological Phases from a Dynamical Gauge Field,” *Physical Review Letters* **129**, 180401 (2022).
- [15] Kohei Kawabata, Ken Shiozaki, and Shinsei Ryu, “Many-body topology of non-Hermitian systems,” *Physical Review B* **105**, 165137 (2022).
- [16] Tsuneya Yoshida and Yasuhiro Hatsugai, “Fate of exceptional points under interactions: Reduction of topological classifications,” *Physical Review B* **107**, 075118 (2023).
- [17] Tsuneya Yoshida, Koji Kudo, Hosho Katsura, and Yasuhiro Hatsugai, “Fate of fractional quantum Hall states in open quantum systems: Characterization of correlated topological states for the full Liouvillian,” *Physical Review Research* **2**, 033428 (2020).
- [18] Henry Shackleton and Mathias S. Scheurer, “Protection of parity-time symmetry in topological many-body systems: Non-Hermitian toric code and fracton models,” *Physical Review Research* **2**, 033022 (2020).
- [19] Masaya Nakagawa, Norio Kawakami, and Masahito Ueda, “Exact liouvillian spectrum of a one-dimensional dissipative hubbard model,” *Physical Review Letters* **126**, 110404 (2021).
- [20] Kazuki Yamamoto, Masaya Nakagawa, Masaki Tezuka, Masahito Ueda, and Norio Kawakami, “Universal properties of dissipative Tomonaga-Luttinger liquids: Case study of a non-Hermitian XXZ spin chain,” *Physical Review B* **105**, 205125 (2022).
- [21] To precisely hit the exception point, we set t_2 to the value of 0.9606414797204921 in double-precision.
- [22] See Supplemental Material at [URL will be inserted by publisher] for the biorthonormal form of wave functions for eigenstates (1), block diagonalization of the non-Hermitian reduced density matrix (2) using well-made instruction recipes, perturbation results of the model (4), and benchmarks in other commonly encountered models, which includes Refs. [10, 20, 37, 40, 41, 50–60].
- [23] Steven R. White, “Density matrix formulation for quantum renormalization groups,” *Physical Review Letters* **69**, 2863 (1992).
- [24] Xiaoqun Wang and Tao Xiang, “Transfer-matrix density-matrix renormalization-group theory for thermodynamics of one-dimensional quantum systems,” *Physical Review B* **56**, 5061 (1997).
- [25] Kenneth G. Wilson, “The renormalization group and critical phenomena,” *Reviews of Modern Physics* **55**, 583 (1983).
- [26] Ali Mostafazadeh, “Pseudo-Hermiticity versus PT symmetry: The necessary condition for the reality of the spectrum of a non-Hermitian Hamiltonian,” *Journal of Mathematical Physics* **43**, 205 (2002).
- [27] Malte Henkel and Ulrich Schollwöck, “Universal finite-size scaling amplitudes in anisotropic scaling,” *Journal of Physics A: Mathematical and General* **34**, 3333–3350 (2001).
- [28] Ian Affleck, Walter Hofstetter, David R Nelson, and Ulrich Schollwöck, “Non-hermitian luttinger liquids and flux line pinning in planar superconductors,” *Journal of Statistical Mechanics: Theory and Experiment* **2004**, P10003 (2004).
- [29] Enrico Carlon, Malte Henkel, and Ulrich Schollwöck, “Critical properties of the reaction-diffusion model $2 \vec{A} \rightarrow 3a, 2 \vec{A} \rightarrow 0$,” *Physical Review E* **63**, 036101 (2001).
- [30] Yasuhiro Hieida, “Application of the density matrix renormalization group method to a non-equilibrium problem,” *Journal of the Physical Society of Japan* **67**, 369–372 (1998).
- [31] Kristan Temme and Frank Verstraete, “Stochastic matrix product states,” *Physical Review Letters* **104**, 210502 (2010).
- [32] T. H. Johnson, T. J. Elliott, S. R. Clark, and D. Jaksch, “Capturing exponential variance using polynomial resources: Applying tensor networks to nonequilibrium stochastic processes,” *Physical Review Letters* **114**, 090602 (2015).
- [33] Ian N. Zwaan and Michiel E. Hochstenbach, “Krylov–Schur-Type Restarts for the Two-Sided Arnoldi Method,” *SIAM Journal Matrix Analysis Applications* **38**, 297 (2017).
- [34] Dorje C Brody, “Biorthogonal quantum mechanics,” *Journal of Physics A: Mathematical and Theoretical* **47**, 035305 (2013).
- [35] Yu-Kun Huang, “Biorthonormal transfer-matrix renormalization-group method for non-Hermitian matrices,” *Physical Review E* **83**, 036702 (2011).
- [36] U. Schollwöck, “The density-matrix renormalization group,” *Reviews of Modern Physics* **77**, 259 (2005).
- [37] L. Mirsky, “A trace inequality of John von Neumann,” *Monatshefte für Mathematik* **79**, 303 (1975).
- [38] J. Ignacio Cirac, David Pérez-García, Norbert Schuch, and Frank Verstraete, “Matrix product states and projected entangled pair states: Concepts, symmetries, theorems,” *Reviews of Modern Physics* **93**, 045003 (2021).
- [39] Ivan Markovskiy, “Structured low-rank approximation and its applications,” *Automatica* **44**, 891 (2008).
- [40] Andreas Honecker, Shijie Hu, Robert Peters, and Johannes Richter, “Dynamic and thermodynamic properties of the generalized diamond chain model for azurite,” *Journal of Physics: Condensed Matter* **23**, 164211 (2011).
- [41] Shijie Hu, B. Normand, Xiaoqun Wang, and Lu Yu, “Accurate determination of the gaussian transition in spin-1 chains with single-ion anisotropy,” *Physical Review B* **84**, 220402(R) (2011).
- [42] Shi-Jian Gu, Ho-Man Kwok, Wen-Qiang Ning, and Hai-Qing Lin, “Fidelity susceptibility, scaling, and universality in quantum critical phenomena,” *Physical Review B* **77**, 245109 (2008).
- [43] Faisal Alsallom, Loïc Herviou, Oleg V. Yazyev, and Marta Brzezińska, “Fate of the non-hermitian skin effect in many-body fermionic systems,” *Physical Review Research* **4**, 033122 (2022).
- [44] M. S. Rudner and L. S. Levitov, “Topological transition in a non-hermitian quantum walk,” *Physical Review Letters* **102**, 065703 (2009).
- [45] Shunyu Yao and Zhong Wang, “Edge States and Topological Invariants of Non-Hermitian Systems,” *Physical Review Letters* **121**, 086803 (2018).
- [46] Naomichi Hatano and David R. Nelson, “Localization transitions in non-hermitian quantum mechanics,” *Phys-*

- ical Review Letters **77**, 570–573 (1996).
- [47] Zhen Guo, Zheng-Tao Xu, Meng Li, Li You, and Shuo Yang, “Variational matrix product state approach for non-hermitian system based on a companion hermitian hamiltonian,” *arXiv preprint arXiv:2210.14858* (2022), 10.48550/ARXIV.2210.14858.
- [48] Guangze Chen, Fei Song, and Jose L. Lado, “Topological spin excitations in non-hermitian spin chains with a generalized kernel polynomial algorithm,” *Physical Review Letters* **130**, 100401 (2023).
- [49] Xue-Jia Yu, Zhiming Pan, Limei Xu, and Zi-Xiang Li, “Non-hermitian strongly interacting dirac fermions: a quantum monte-carlo study,” *arXiv preprint arXiv:2302.10115* (2023), 10.48550/ARXIV.2302.10115.
- [50] Ulrich Schollwöck, “The density-matrix renormalization group in the age of matrix product states,” *Annals of Physics January 2011 Special Issue*, **326**, 96–192 (2011).
- [51] Xian-Da Zhang, *Matrix Analysis and Applications* (Cambridge University Press, 2017).
- [52] Moody T. Chu, Robert E. Funderlic, and Robert J. Plemmons, “Structured low rank approximation,” *Linear Algebra and its Applications* **366**, 157 (2003).
- [53] Zhaojun Bai and James W. Demmel, “On swapping diagonal blocks in real schur form,” *Linear Algebra and its Applications* **186**, 75–95 (1993).
- [54] Robert E. Hartwig, “Roth’s removal rule revisited,” *Linear Algebra and its Applications* **49**, 91–115 (1983).
- [55] R. H. Bartels and G. W. Stewart, “Algorithm 432 [c2]: Solution of the matrix equation $ax + xb = c$ [f4],” *Communications of the ACM* **15**, 820–826 (1972).
- [56] L. Kohaupt, “Introduction to a gram-schmidt-type biorthogonalization method,” *Rocky Mountain Journal of Mathematics* **44**, 1265 (2014).
- [57] Jon Wilkening, “An algorithm for computing Jordan chains and inverting analytic matrix functions,” *Linear Algebra and its Applications* **427**, 6–25 (2007).
- [58] M. Takahashi, “Half-filled Hubbard model at low temperature,” *Journal of Physics C: Solid State Physics* **10**, 1289–7301 (1977).
- [59] Frédéric Mila and Kai Phillip Schmidt, “Strong-Coupling Expansion and Effective Hamiltonians,” in *Introduction to Frustrated Magnetism: Materials, Experiments, Theory*, Springer Series in Solid-State Sciences, edited by Claudine Lacroix, Philippe Mendels, and Frédéric Mila (Springer, Berlin, Heidelberg, 2011) pp. 537–559.
- [60] Simon Lieu, “Topological phases in the non-Hermitian Su-Schrieffer-Heeger model,” *Physical Review B* **97**, 045106 (2018).

Supplemental Material for: Density-matrix renormalization group algorithm for non-Hermitian systems

Peigeng Zhong,¹ Wei Pan,^{1,2} Haiqing Lin,^{3,1,*} Xiaoqun Wang,^{3,†} and Shijie Hu^{1,‡}

¹Beijing Computational Science Research Center, Beijing 100084, China

²Department of Physics, Beijing Normal University, Beijing, 100875, China

³School of Physics, Zhejiang University, Hangzhou, 310058, China

This supplemental material provides an in-depth description of the density matrix renormalization group algorithm and biorthogonal physics. Our discussion covers several topics, including the biorthonormal form of wave functions for eigenstates, block diagonalization of the non-Hermitian reduced density matrix using well-made instruction recipes, perturbation results of the model outlined in the main text, and benchmarks in other commonly encountered models.

I. BIORTHONORMAL FORM

When we divide/partition a chain of L sites into two semi-chains, the left one (\triangleleft) with n_{\triangleleft} sites and the right one (\triangleangleright) with n_{\triangleangleright} sites, respectively, the left eigenstate $\langle\bar{\Psi}|$ and the right eigenstate $|\Psi\rangle$ of the non-Hermitian Hamiltonian H can be expressed as

$$\langle\bar{\Psi}| = \sum_{\alpha,\alpha'} \langle\bar{y}_{\alpha}| \bar{\Theta}_{\alpha,\alpha'} \langle\bar{z}_{\alpha'}| = \begin{array}{c} \bar{Y} \\ \alpha \\ \diamond \\ \bar{Z} \\ \alpha' \\ \bar{\Theta} \end{array}, \quad |\Psi\rangle = \sum_{\alpha,\alpha'} |y_{\alpha}\rangle \Theta_{\alpha,\alpha'} |z_{\alpha'}\rangle = \begin{array}{c} \tau_{\triangleleft} \\ Y \\ \alpha \\ \diamond \\ Z \\ \alpha' \\ \Theta \\ \tau_{\triangleangleright} \end{array}, \quad (1)$$

where $\tau_{\triangleleft,\triangleangleright}(\alpha, \alpha')$ represent the physical (bond) indices for two semi-chains. A bare basis $|\tau_{\triangleleft,\triangleangleright}\rangle$ is a product of local physical bases $|\tau_{\ell}\rangle$, i.e., $|\tau_{\triangleleft}\rangle = \otimes_{\ell=1}^{n_{\triangleleft}} |\tau_{\ell}\rangle$ and $|\tau_{\triangleangleright}\rangle = \otimes_{\ell=n_{\triangleleft}+1}^L |\tau_{\ell}\rangle$. Similarly, $\langle\tau_{\triangleleft}| = \otimes_{\ell=1}^{n_{\triangleleft}} \langle\tau_{\ell}|$ and $\langle\tau_{\triangleangleright}| = \otimes_{\ell=n_{\triangleleft}+1}^L \langle\tau_{\ell}|$. We assume that the Hilbert spaces for the left and right semi-chains have dimensions of d^{\triangleleft} and d^{\triangleangleright} , respectively. Thus, the dimension of the whole Hilbert space in which the Hamiltonian H lives is given by $d^{\text{T}} = d^{\triangleleft}d^{\triangleangleright}$. The transformed bases

$$\langle\bar{y}_{\alpha}| = \sum_{\tau_{\triangleleft}} \bar{Y}_{\alpha,\tau_{\triangleleft}} \langle\tau_{\triangleleft}|, \quad \langle\bar{z}_{\alpha'}| = \sum_{\tau_{\triangleangleright}} \bar{Z}_{\alpha',\tau_{\triangleangleright}} \langle\tau_{\triangleangleright}|, \quad |y_{\alpha}\rangle = \sum_{\tau_{\triangleleft}} |\tau_{\triangleleft}\rangle Y_{\tau_{\triangleleft},\alpha}, \quad |z_{\alpha'}\rangle = \sum_{\tau_{\triangleangleright}} |\tau_{\triangleangleright}\rangle Z_{\tau_{\triangleangleright},\alpha'}, \quad (2)$$

can be written as superpositions of the bare bases $|\tau_{\triangleleft,\triangleangleright}\rangle$.

These bases should satisfy the biorthonormalization condition: $\langle\bar{y}_{\alpha}|y_{\alpha'}\rangle = \langle\bar{z}_{\alpha}|z_{\alpha'}\rangle = \delta_{\alpha,\alpha'}$. As a result, the transformation matrices \bar{Y} , Y , \bar{Z} and Z fulfill the left and right biorthonormalization conditions (LBC and RBC), respectively, as follows by

$$\text{LBC: } \bar{Y}Y = \begin{array}{c} \bar{Y} \\ \hline Y \end{array} = \mathbb{1}, \quad \text{RBC: } \bar{Z}Z = \begin{array}{c} \bar{Z} \\ \hline Z \end{array} = \mathbb{1}, \quad (3)$$

which implies that $\bar{Y} = Y^{-1}$ and $\bar{Z} = Z^{-1}$. Eq. (1) indicates the decompositions of $\langle\bar{\Psi}|$ and $|\Psi\rangle$ in terms of \bar{Y} , \bar{Z} , Y and Z in the *biorthonormal form*. The reduced density matrix for the left semi-chain is given by

$$\rho = \text{tr}_{\triangleangleright} |\Psi\rangle\langle\bar{\Psi}| = \begin{array}{c} \bar{Y} \\ \hline Y \end{array} \begin{array}{c} \bar{\Theta} \\ \hline \Theta \end{array} \begin{array}{c} \bar{Z} \\ \hline Z \end{array} = \begin{array}{c} \bar{Y} \\ \hline Y \end{array} \begin{array}{c} \bar{\Theta} \\ \hline \Theta \end{array}, \quad (4)$$

which is generally non-Hermitian. Due to the normalization condition $\langle\bar{\Psi}|\Psi\rangle = 1$, it is easy to verify that $\text{tr}_{\triangleleft}\rho = 1$. Since the biorthonormalization condition $\bar{Y}Y = \mathbb{1}$, the spectrum of ρ is identical to that of $\bar{\Theta}\Theta^{\text{T}}$, which validates the notion that Θ ($\bar{\Theta}$) represents the wave function $|\Psi\rangle$ ($\langle\bar{\Psi}|$) under the transformed bases. The superscript “ T ” denotes the “transpose” operation.

In the renormalization group (RG) procedure of bbDMRG, which will be discussed in the next section, certain transformed bases are removed. As a result, \bar{Y} (\bar{Z}) is no longer the inverse matrix of Y (Z). In addition, in contrast

to the typical matrix product state representation [1], both matrices $\bar{\Theta}$ and Θ are generally not diagonal for non-Hermitian systems.

By performing the decomposition recursively, the eigenstate $\langle \bar{\Psi} |$ and $|\Psi\rangle$ can be expressed in a nested form. Specifically,

$$\begin{aligned} \langle \bar{\Psi} | &= \sum_{\tau_{\triangleleft}, \tau_{\triangleright}} \langle \tau_{\triangleleft} | (\bar{Y}_1 \cdots \bar{Y}_{n_{\triangleleft}} \bar{\Theta} \bar{Z}_{n_{\triangleright}} \cdots \bar{Z}_1)_{\tau_{\triangleleft}, \tau_{\triangleright}} \langle \tau_{\triangleright} | = \begin{array}{c} \bar{Y}_1 \cdots \bar{Y}_{n_{\triangleleft}} \bar{\Theta} \bar{Z}_{n_{\triangleright}} \cdots \bar{Z}_1 \\ \tau_1 \quad \tau_{n_{\triangleleft}} \quad \tau_{n_{\triangleleft}+1} \quad \tau_L \end{array}, \\ |\Psi\rangle &= \sum_{\tau_{\triangleleft}, \tau_{\triangleright}} |\tau_{\triangleleft}\rangle (Y_1 \cdots Y_{n_{\triangleleft}} \Theta Z_{n_{\triangleright}} \cdots Z_1)_{\tau_{\triangleleft}, \tau_{\triangleright}} |\tau_{\triangleright}\rangle = \begin{array}{c} Y_1 \cdots Y_{n_{\triangleleft}} \Theta Z_{n_{\triangleright}} \cdots Z_1 \\ \tau_1 \quad \tau_{n_{\triangleleft}} \quad \tau_{n_{\triangleleft}+1} \quad \tau_L \end{array}. \end{aligned} \quad (5)$$

Each pair of transformation matrices \bar{Y}_ℓ (\bar{Z}_ℓ) and Y_ℓ (Z_ℓ) with $\ell \geq 2$ satisfies the local LBC and RBC, i.e.,

$$\text{LBC: } \bar{Y}_\ell Y_\ell = \begin{array}{c} \bar{Y}_\ell \\ | \\ Y_\ell \end{array} = \mathbb{1}, \quad \text{RBC: } \bar{Z}_\ell Z_\ell = \begin{array}{c} \bar{Z}_\ell \\ | \\ Z_\ell \end{array} = \mathbb{1}. \quad (6)$$

Using a standard technique of singular value decomposition (SVD) [1], the biorthonormal form of the decompositions of the eigenstates $\langle \bar{\Psi} |$ and $|\Psi\rangle$ can be conveniently transformed into a canonical one without sacrificing accuracy, which allows us to carry out the right-right (RR) measurement of the physical operators as defined in the main text.

II. NON-HERMITIAN REDUCED DENSITY MATRIX

In this section, we construct the transformation matrix derived from the reduced density matrix for the left semi-chain $\rho = \text{tr}_{\triangleright} |\Psi\rangle\langle \bar{\Psi}|$ and present the estimates of the errors resulting from the truncation of the Hilbert space representing the biorthonormal form of the eigenstates. The discussion applies equally to the right semi-chain.

A. Jordan normal form

For non-Hermitian ρ (any matrix in mathematics), a Jordan normal form J , consisting of n_J Jordan blocks, can be obtained through a generalized eigenvalue decomposition (GEVD), given by

$$\rho = Y J \bar{Y} = \sum_{k=1}^{n_J} \sum_{\beta, \beta'=1}^{r_k} y_{\beta}^{(k)} J_{\beta, \beta'}^{(k)} \bar{y}_{\beta'}^{(k)}, \quad (7)$$

where $\bar{y}_{\beta}^{(k)}$ and $y_{\beta}^{(k)}$ are the left and right *generalized* eigenvectors of ρ , respectively. The Jordan block index k varies from 1 to n_J , and the inner index β runs over the range $[1, r_k]$. r_k denotes the dimension of the k -th Jordan block, which is equal to the rank of the block. Consequently, the total dimension of the Hilbert space for the left semi-chain is given by $d^{\triangleleft} = \sum_{k=1}^{n_J} r_k$. In the k -th block, the matrix elements $J_{\beta, \beta}^{(k)} = \zeta_k$ and $J_{\beta, \beta+1}^{(k)} = 1$, while all other elements are zero. The complex number ζ_k represents the uniform eigenvalue for the k -th block.

In the case of diagonalizable ρ , where $r_k = 1$ for all k , we can write $\rho = \sum_{k=1}^{n_J} y_1^{(k)} \zeta_k \bar{y}_1^{(k)}$ using an eigenvalue decomposition (EVD), where $\bar{y}_1^{(k)}$ and $y_1^{(k)}$ are the left and right eigenvectors of ρ . The eigenvalues of the diagonalizable reduced density matrix are related to the wave functions in the transformed bases in a simple way, resulting in $\Theta \bar{\Theta}^{\top} = \zeta$.

For the sake of convenience in the upcoming discussions, we establish a convention. This convention involves the transformation of a binary index (k, β) , which comprises a Jordan block index k and an inner index β , into a regular single-element index $\alpha = \beta + \sum_{k'=1}^{k-1} r_{k'}$. A representative example depicting this convention is illustrated in Fig. 1.

When the truncation dimension m for the bond index is small, we only select the first m (generalized) eigenvector pairs to optimally construct the saved space (s) and use the rest $d^{\triangleleft} - m$ pairs to build up the discarded space (d). The saved space is actually the renormalized Hilbert space for the left semi-chain, which corresponds to the first K_r Jordan blocks. Thus, the truncation dimension is also given by $m = \sum_{k=1}^{K_r} r_k$. $\bar{Y} = (\bar{Y}^{(s)\top} \bar{Y}^{(d)\top})^{\top}$ and $Y = (Y^{(s)} Y^{(d)})$ represent two $d^{\triangleleft} \times d^{\triangleleft}$ transformation matrices, respectively, i.e.,

$$\bar{Y}^{(s)} = (\bar{y}_1^{\top} \cdots \bar{y}_m^{\top})^{\top}, \quad \bar{Y}^{(d)} = (\bar{y}_{m+1}^{\top} \cdots \bar{y}_{d^{\triangleleft}}^{\top})^{\top}, \quad Y^{(s)} = (y_1 \cdots y_m), \quad Y^{(d)} = (y_{m+1} \cdots y_{d^{\triangleleft}}). \quad (8)$$

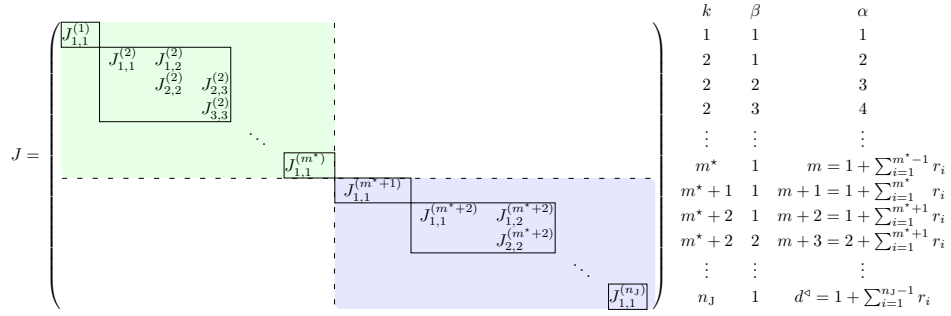


FIG. 1. Applying GEVD to the reduced density matrix ρ for the left semi-chain yields a Jordan normal form J consisting of n_J Jordan blocks $J^{(k)}$. On the right-hand side, we demonstrate the binary index (k, β) for the generalized eigenvector pair of $\bar{y}_\beta^{(k)}$ and $y_\beta^{(k)}$, labeled by a Jordan block index k and an inner index β , as well as the equivalent single-element index α . To construct the saved space (blocks with a green shaded background), we use the first m pairs of the left eigenvectors $\bar{y}_1, \dots, \bar{y}_m$ and the right eigenvectors y_1, \dots, y_m , corresponding to the first K_r Jordan blocks. The remaining $d^\natural - m$ pairs of $\bar{y}_{m+1}, \dots, \bar{y}_{d^\natural}$ and $y_{m+1}, \dots, y_{d^\natural}$ (blocks with a blue shaded background) are discarded.

In Eq. (8), \bar{y}_α is a d^\natural -dimensional row vector, i.e., $1 \times d^\natural$ matrix, and y_α is a $d^\natural \times 1$ matrix, so $\bar{Y}^{(s)}$ is an $m \times d^\natural$ matrix, $Y^{(s)}$ is a $d^\natural \times m$ matrix, $\bar{Y}^{(d)}$ is a $(d^\natural - m) \times d^\natural$ matrix, and $Y^{(d)}$ is a $d^\natural \times (d^\natural - m)$ matrix. Therefore,

$$\rho = \rho^{(s)} + \rho^{(d)} = \begin{pmatrix} Y^{(s)} & Y^{(d)} \end{pmatrix} \begin{pmatrix} B^{(s)} & 0 \\ 0 & B^{(d)} \end{pmatrix} \begin{pmatrix} \bar{Y}^{(s)} \\ \bar{Y}^{(d)} \end{pmatrix}, \quad (9)$$

where the Jordan normal form J can be expressed as the direct sum of two subblocks: $B^{(s)} = \bar{Y}^{(s)} \rho^{(s)} Y^{(s)}$ and $B^{(d)} = \bar{Y}^{(d)} \rho^{(d)} Y^{(d)}$, as shown in Fig. 1. Here, $\rho^{(s)}$ and $\rho^{(d)}$ are $d^\natural \times d^\natural$ matrices, with $B^{(s)}$ being an $m \times m$ matrix and $B^{(d)}$ being a $(d^\natural - m) \times (d^\natural - m)$ matrix. Moreover, we have

$$\rho^{(s)} = Y^{(s)} B^{(s)} \bar{Y}^{(s)}, \quad \rho^{(d)} = Y^{(d)} B^{(d)} \bar{Y}^{(d)}. \quad (10)$$

B. Upper bounds for the measurement errors

When the left and right eigenvectors of $\rho^{(s)}$ are employed to renormalize the Hilbert space and the corresponding operators, the error for the left-right (LR) measurement of a physical operator O in matrix representation can be determined as follows:

$$\varepsilon = |\text{tr}_d(\rho O) - \text{tr}_d(\rho^{(s)} O)| = |\text{tr}_d(\rho^{(d)} O)|. \quad (11)$$

After the SVDs of $\rho^{(d)}$ and O are executed, and both singular values $\lambda_\alpha^{\rho^{(d)}}$ and λ_α^O are sorted in descending order, an upper bound (UB) $\varepsilon_1 = \sum_\alpha \lambda_\alpha^{\rho^{(d)}} \lambda_\alpha^O \geq \varepsilon$ can be obtained using von Neumann's trace inequality [2]. As $\lambda_1^{\rho^{(d)}} \geq \lambda_2^{\rho^{(d)}} \geq \dots \geq \lambda_{d^\natural}^{\rho^{(d)}}$, a larger UB, ε_2 , can be found, that is,

$$\varepsilon_2 = a \max_{\alpha \in [1, d^\natural]} \{\lambda_\alpha^{\rho^{(d)}}\} = a \lambda_1^{\rho^{(d)}} \geq \varepsilon_1, \quad (12)$$

where $a = \sum_\alpha \lambda_\alpha^O$. One also has

$$\max_{\alpha \in [1, d^\natural]} \{\lambda_\alpha^{\rho^{(d)}}\} = \|\rho^{(d)}\|_2, \quad (13)$$

where the 2-norm [3] is naturally defined as $\|O\|_2 = \sup_v (\|Ov\|_2 / \|v\|_2)$ with v being any non-null d^\natural -dimension column vector.

According to the Eckart-Young-Mirsky theorem [3], the optimal representation of a matrix Q with rank r in terms of approximate matrices $\{Q_a\}$ with rank m , denoted as Q_a^{opt} , can be achieved if and only if the variance of $\|Q - Q_a\|_2$ is minimized. This goal is achieved in two steps. First, implement the SVD of $Q = U^Q \lambda^Q V^{Q\dagger}$, where two

unitary matrices U^Q and V^Q represent the left and right singular vectors, respectively. Secondly, the left and right singular vectors corresponding to the largest m singular values are used to construct Q_a . So, the optimal solution is $Q_a^{\text{opt}} = U^Q \text{diag}(\lambda_1^Q, \dots, \lambda_m^Q, 0, \dots, 0) V^{Q\dagger}$ with $m \leq r$.

The Eckart-Young-Mirsky theorem provides a method for constructing the saved space simply using the singular vectors corresponding to the largest m singular values. This approach allows us to minimize $\|\rho^{(d)}\|_2 = \|\rho - \rho^{(s)}\|_2$ and reach the minimum value of λ_{m+1}^p . In terms of terminology, we refer to $\rho^{(s)}$ as the best *low-rank approximation* of ρ . In those matrix-product-state/tensor algorithms for the Hermitian Hamiltonians that inherently allow the left Hilbert space $\bar{\mathcal{H}}$ to be the adjoint of the right one \mathcal{H} . Consequently, the SVD of the Hermitian ρ is equivalent to its EVD originally adapted in DMRG.

However, in the non-unitary RG procedure for non-Hermitian Hamiltonians, $\bar{\mathcal{H}}$ is no longer the adjoint of \mathcal{H} so that the left and right bases are renormalized by \bar{Y} and Y , respectively. In this case, the operators are biorthonormally renormalized by \bar{Y} and Y . According to Eq. (10), (12) and (13), the minimization of

$$\varepsilon_2 = a\|\rho^{(d)}\|_2 = a\|YB^{(d)}\bar{Y}\|_2 \quad (14)$$

can be further considered by the so-called *structured low-rank approximation*. Mathematically, however, it is still an NP-hard problem [4]. To address this problem, the Cauchy-Schwarz inequality allows us to introduce a larger UB ε_3

$$\varepsilon_2 \leq a\|Y\|_2\|B^{(d)}\|_2\|\bar{Y}\|_2 = a\kappa\|B^{(d)}\|_2 = a\kappa \max_{k \in [K_r+1, n_J]} \|J^{(k)}\|_2 = \varepsilon_3. \quad (15)$$

where $\kappa = \|Y\|_2\|\bar{Y}\|_2$ is called the condition number, measuring the strength on the deviation of the non-Hermiticity on ρ from the optimal approximation of all possible Hermitian ones, or the deviation of the transformation matrix away from the optimal unitary one. While $\kappa = 1$ for the unitary case, but it is often large and even becomes $\kappa \gg 1$ for non-Hermitian cases, which can lead to numerical instability of RG procedures. In the following subsection, we will discuss the techniques to reduce the condition number κ by introducing the redundant degrees of freedom in the saved space, which is important to ensure the accuracy of bbDMRG.

For the k -th Jordan block $J^{(k)}$, we define a weight w_k as $\|J^{(k)}\|_2$, which gives rise to the following bounds

$$|\zeta_k| \leq w_k \leq |\zeta_k| + 1 \quad (16)$$

where the left and right equal signs in the above inequality hold for $r_k = 1$ and ∞ , respectively. Practically, we take w_k as the weight analogous to the eigenvalue of the reduced density matrix in the conventional DMRG. This weight helps us to assess the importance of the (generalized) eigenvectors corresponding to the k -th Jordan blocks, in order to decide whether to keep or discard these vectors for the Hilbert space truncation in the RG procedure. Hereafter, the truncation error is estimated by $\varepsilon_t = \sum_{k=K_r+1}^{n_J} w_k$ for the non-Hermitian case.

In summary, we establish a theory of a truncation criterion for the non-Hermitian RG procedure: Suppose that $B^{(s)}$ and $B^{(d)}$ have weight spectra $w^{(s)}$ and $w^{(d)}$ sorted in descending order, and $w_{\min}^{(s)} > w_{\max}^{(d)}$ represent the minimum and maximum weights in the spectra $w^{(s)}$ and $w^{(d)}$, respectively. Thus $\rho^{(s)}$ can be considered as the *best* structured low-rank approximation of ρ , for which the error UB for the RG procedure is at most $\varepsilon_3 = a\kappa w_{\max}^{(d)} = a\kappa w_{m+1} \geq \varepsilon_2 \geq \varepsilon_1$. The condition number κ depends on the practical choices of Y and \bar{Y} .

C. Techniques for numerical stability

In the non-unitary RG procedure, we notice that the transformation matrices \bar{Y} and Y in Eq. (9) are not unique. One can apply an $m \times m$ invertible matrix η to the saved space and obtain a new representation of the Hilbert space for ρ by

$$\bar{Y}_\eta^{(s)} = \eta^{-1} \bar{Y}^{(s)}, \quad Y_\eta^{(s)} = Y^{(s)} \eta, \quad (17)$$

so that $\bar{Y} = (\bar{Y}_\eta^{(s)\top} \bar{Y}^{(d)\top})^\top$ and $Y = (Y_\eta^{(s)} Y^{(d)})$. In this case, ρ can be still expressed in terms of the following block-diagonal form of B_η , that is,

$$\rho = Y_\eta B_\eta \bar{Y}_\eta = \begin{pmatrix} Y_\eta^{(s)} & Y^{(d)} \end{pmatrix} \begin{pmatrix} B_\eta^{(s)} & 0 \\ 0 & B^{(d)} \end{pmatrix} \begin{pmatrix} \bar{Y}_\eta^{(s)} \\ \bar{Y}^{(d)} \end{pmatrix}. \quad (18)$$

This provides a kind of redundant degrees of freedom in finding the optimal $Y^{(s)}$ and $\bar{Y}^{(s)}$, which allows us to effectively reduce the condition number $\kappa = \|\bar{Y}_\eta\|_2 \|Y_\eta\|_2$ so as to suppress the numerical instability. In this case, the subblock $B_\eta^{(s)} = \bar{Y}_\eta^{(s)} \rho Y_\eta^{(s)} = \eta^{-1} B^{(s)} \eta$ may become dense, but the truncation error ϵ_t obviously remains unaffected by the choice of η .

In general, it is not possible to reliably obtain the paired transformation matrices Y and \bar{Y} by a full diagonalization of ρ when κ is large. Moreover, one cannot know the information about κ before determining Y and \bar{Y} .

Fortunately, we find that it is feasible to take a two-step approach to implement the block diagonalization of ρ . First, we use Schur decomposition to convert ρ into its upper triangular form, whose diagonal element corresponds to the eigenvalue ζ_k . In this step, we sort bases in descending order of $|\zeta_k|$ by direct swapping [5]. After that, the full space of the representation of ρ has been partitioned into the saved space and the discarded space done and mentioned above. In this case, ρ can be expressed as

$$\rho = \begin{pmatrix} S^{(s)} & S^{(d)} \end{pmatrix} \begin{pmatrix} A & D \\ \mathbb{0} & C \end{pmatrix} \begin{pmatrix} S^{(s)\dagger} \\ S^{(d)\dagger} \end{pmatrix}, \quad (19)$$

which $S = \begin{pmatrix} S^{(s)} & S^{(d)} \end{pmatrix}$ is a unitary matrix, both the $m \times m$ matrix A and the $(d^s - m) \times (d^s - m)$ matrix B are the upper triangular matrices, and C is an $m \times (d^s - m)$ dense rectangular matrix. We then use Roth's removal rule [6] to obtain a similarity transformation that converts the upper triangular matrix into a block diagonal form as follows

$$\begin{pmatrix} \mathbb{1} & X \\ \mathbb{0} & \mathbb{1} \end{pmatrix} \begin{pmatrix} A & D \\ \mathbb{0} & C \end{pmatrix} \begin{pmatrix} \mathbb{1} & -X \\ \mathbb{0} & \mathbb{1} \end{pmatrix} = \begin{pmatrix} A & \mathbb{0} \\ \mathbb{0} & C \end{pmatrix} \quad (20)$$

where X is a unique solution of the Sylvester equation $AX - XC = D$ [7]. If A and C have different eigenvalues, as in Eq. (19), X can be efficiently obtained using the Bartels-Stewart algorithm [7]. In terms of A , C , S and X , the block diagonalization of ρ is thus expressed as

$$\rho = \begin{pmatrix} S^{(s)} & S^{(d)} - S^{(s)}X \end{pmatrix} \begin{pmatrix} A & \mathbb{0} \\ \mathbb{0} & C \end{pmatrix} \begin{pmatrix} S^{(s)\dagger} + XS^{(d)\dagger} \\ S^{(d)\dagger} \end{pmatrix}, \quad (21)$$

which gives rise to $\bar{Y}^{(s)} = S^{(s)\dagger} + XS^{(d)\dagger}$, $\bar{Y}^{(d)} = S^{(d)\dagger}$, $Y^{(s)} = S^{(s)}$, $Y^{(d)} = S^{(d)} - S^{(s)}X$, $B^{(s)} = A$ and $B^{(d)} = C$. Up to this point, it is still encouraging to simultaneously transform $Y^{(s)}$ and $\bar{Y}^{(s)}$ by empirically choosing appropriate η to further reduce κ . To provide some guidelines, we elucidate six relevant cases, some of which remarkably suppress κ and improve the numerical stability. Especially the instructions are given for the last two cases where we have to face the brutal-force GEVD of ρ .

(1) Normal matrix. If ρ is normal, which means that $[\rho, \rho^\dagger] = 0$, both ρ and ρ^\dagger can be diagonalized using the same unitary matrix U [3]. One can simply take $\bar{Y} = U^\dagger$ and $Y = U$ so that $\bar{Y}Y = \mathbb{1}$, and U can be obtained by diagonalizing the Hermitian matrix $(\rho + \rho^\dagger)/2$. The hybridization of ρ and ρ^\dagger allows for a seamless connection to the DMRG method for the Hermitian Hamiltonian. In this case, $\kappa = 1$ automatically.

(2) Null space. For a null space \emptyset , zero eigenvalues $\zeta = 0$ are in the presence, along with the left vectors \bar{y} and right vectors y . Thus, we get $\rho y = 0$ and $\bar{y} \rho = 0$. Alternatively, orthonormal bases of ρ can be obtained by using the ‘‘null’’ subroutine in MATLAB. This subroutine implements the SVD of ρ and solves $\rho v^\rho = \lambda^\rho u^\rho$, where u^ρ and v^ρ are two singular vectors, and the corresponding singular value $\lambda^\rho = 0$ mathematically. In numerical practice, those vectors with singular values smaller than a tiny threshold ϵ form an orthonormal basis set for the null space \emptyset of the dimension d^\emptyset , spanned as

$$U^\emptyset = (u_1^\rho \ \cdots \ u_{d^\emptyset}^\rho) \quad \text{and} \quad V^\emptyset = (v_1^\rho \ \cdots \ v_{d^\emptyset}^\rho). \quad (22)$$

from which one can form a matrix $T = V^{\emptyset\dagger} U^\emptyset$. Using an EVD in the standard LAPACK library, one has $T = CEC^{-1}$, where C is an invertible matrix in terms of eigenvectors of T , and E is a diagonal matrix consisting of corresponding eigenvalues e_α with $\alpha = 1, \dots, d^\emptyset$. Eventually, in terms of u^ρ , v^ρ , C , C^{-1} and E , one obtains biorthonormalized left and right vectors

$$\bar{y}_\alpha = \sum_{\alpha'} E_{\alpha,\alpha'}^{-1/2} C_{\alpha,\alpha'}^{-1} v_{\alpha'}^\dagger \quad \text{and} \quad y_\alpha = \sum_{\alpha'} u_{\alpha'} C_{\alpha',\alpha} E_{\alpha,\alpha}^{-1/2}, \quad (23)$$

for the null space. The threshold for the tiny eigenvalue in SVD $\epsilon = \epsilon_0 d^s \|\rho\|_\infty / \min |\bar{y}_\alpha y_\alpha|$ typically ranges from 10^{-14} to 10^{-11} in practice, depending on the dimension d^s of ρ , the double-precision limit of floating numbers $\epsilon_0 = 2^{-53} \approx 10^{-16}$, the infinity-norm $\|\rho\|_\infty = \max_{p,p'} |\rho_{p,p'}|$, and the minimal norm of the overlap $\bar{y}_\alpha y_\alpha$.

(3) Biorthonormalization. After obtaining a structured low-rank approximation of ρ , we can numerically improve the biorthonormalization condition by using the Gram-Schmidt-like algorithm [8], which can reduce κ greatly.

(4) Unitarization. When a system is close to an exceptional point (EP) or its eigenstate corresponds to a complex eigenvalue, numerical stability may become a really severe problem, depending on the balance status on biorthonormalization of the left and right \bar{Y} and Y . In this case, one can do some special treatments on the saved space. For the $d^d \times m$ truncated transformation matrix $Y^{(s)}$, one can obtain the SVD of $Y^{(s)} = U^{(s)}\Lambda^{(s)}V^{(s)\dagger}$, where $U^{(s)}$ is a $d^d \times m$ unitary matrix, and $V^{(s)}$ is an $m \times m$ unitary matrix, and $\Lambda^{(s)}$ is an $m \times m$ diagonal matrix. Since $\bar{Y}^{(s)}Y^{(s)} = \mathbb{1}$, we multiply $V^{(s)\dagger}$ and $V^{(s)}$ on both sides of this equation from the left and right directions, respectively. It turns out that

$$V^{(s)\dagger}\bar{Y}^{(s)}U^{(s)}\Lambda^{(s)} = \mathbb{1} . \quad (24)$$

Alternatively, we can express Eq. (24) as $V^{(s)\dagger}\bar{Y}^{(s)\dagger}U^{(s)} = (\Lambda^{(s)})^{-1}$ under the assumption that $\Lambda^{(s)}$ does not contain any zero singular values. If we write that $V^{(s)\dagger}\bar{Y}^{(s)} = (\Lambda^{(s)})^{-1}U^{(s)\dagger} + G$, we obtain $GU^{(s)}\Lambda^{(s)} = 0$ or $GU^{(s)} = 0$, which means that the matrix G is orthogonal to $U^{(s)}$. Neglecting G , we may approximately construct transformation matrices which become unitary,

$$Y'^{(s)} = Y^{(s)}V^{(s)}(\Lambda^{(s)})^{-1} = U^{(s)} \quad \text{and} \quad \bar{Y}'^{(s)} = \Lambda^{(s)}V^{(s)\dagger}\bar{Y}^{(s)} = U^{(s)\dagger} . \quad (25)$$

We note that the above implementation violates the biorthonormalization relation between the saved left vectors in $\bar{Y}^{(s)}$ and the discarded right vectors in $Y^{(d)}$. Consequently, some information from the discarded bases is kept in the saved space, thereby weakening the effectiveness of truncation. In bbDMRG, we evaluate the difference in the lowest energy of the Hamiltonian for the left semi-chain both before and after the RG process. Once the energy difference exceeds a given threshold, we proceed to activate this operation by replacing $\bar{Y}^{(s)}$ and $Y^{(s)}$ with $\bar{Y}'^{(s)}$ and $Y'^{(s)}$, respectively.

(5) Jordan normal form. For the k -th Jordan block with $r_k > 1$, standard libraries such as LAPACK and SciPy offer diagonalization subroutines that can typically be utilized to find the left (generalized) eigenvector $\bar{y}_1^{(k)}$ and the right (generalized) eigenvector $y_1^{(k)}$. However, if other pairs of generalized eigenvectors $\bar{y}_\alpha^{(k)}$ and $y_\alpha^{(k)}$ with $\alpha > 1$ are required, the Jordan-chain algorithm [9] can be employed.

By applying the Jordan-chain recursion, one obtains a sequence of right generalized eigenvectors $y_\alpha^{(k)}$ such as

$$y_\alpha^{(k)} = (\rho - \zeta_k \mathbb{1}) y_{\alpha-1}^{(k)} , \quad (26)$$

for $\alpha = 2, 3, \dots, r_k$. One may then form the right transformation matrix $Y^{(k)} = (y_1^{(k)} \dots y_{r_k}^{(k)})$. Using the Moore–Penrose inverse matrix [3], one obtains the left transformation matrix $\bar{Y}^{(k)}$ as follows:

$$\bar{Y}^{(k)} = P(Y^{(k)})^\dagger , \quad (27)$$

where P is the inverse of the Hermitian matrix $Y^{(k)\dagger}Y^{(k)}$ with rank r_k .

(6) Degeneracy. When the multiplet in the eigenvalue spectrum of ρ emerges, it is possible to reduce condition numbers κ by combining the corresponding eigenvector pairs that have degenerate eigenvalues. To assume that n_d eigenvector pairs share the same eigenvalue, the corresponding left and right eigenvectors live in the $n_d \times n_d$ matrices

$$\bar{Y} = (\bar{y}_1^\dagger \dots \bar{y}_{n_d}^\dagger)^\dagger \quad \text{and} \quad Y = (y_1 \dots y_{n_d}) . \quad (28)$$

Then, we take a generalized QR decomposition of Y , i.e., $Y = QR$ [3], where Q is a unitary matrix and R denotes an upper triangular matrix. The new transformation matrices are thus given by

$$\bar{Y}' = R\bar{Y} \quad \text{and} \quad Y' = Q . \quad (29)$$

where κ becomes smaller.

At the end of the description of techniques details, we note that in the bbDMRG algorithm, the similarity transformation essentially makes the reduced density matrix block diagonal while keeping its eigenvalue spectrum conceptually the same as the true one of GEVD. The spectrum provides the weights in correspondence to the singular values as seen in Fig. 1(e) in the main text, ensuring that the algorithm works well in general. Moreover, in practice, the rescaling of the renormalized Hamiltonians for two semi-chains substantially enhances the efficiency and stability of the DMRG [10] and TMRG [11], which has been used in Fig. 1(f) in the main text.

III. PERTURBATION FOR DOMINANT REPULSION

The main text explores the fascinating non-Hermitian many-body physics, focusing on the scenario of strong repulsion at half-filling. This intriguing situation encompasses several phenomena, including the presence of the non-Hermitian charge density wave (nCDW), the skin effect of a kink observed in the nCDW_k state, and the localization of a kink under the influence of a staggered complex chemical potential. In this context, we provide a perturbation analysis of these phenomena, especially for significantly large V .

A. Effective model

The Hamiltonian for an open Su–Schrieffer–Heeger (SSH) chain of interacting fermions, as defined in Eq. (4) of the main text, can be divided into two parts, i.e., $H = H_0 + H_1$ with $H_0 = H_V$ and $H_1 = H_{t_1} + H_{t_2} + H_u$, where

$$\begin{aligned} H_{t_1} &= \sum_{\ell=1}^N \left(t_L c_{\ell,a}^\dagger c_{\ell,b} + t_R c_{\ell,b}^\dagger c_{\ell,a} \right), & H_{t_2} &= t_2 \sum_{\ell=1}^{N-1} \left(c_{\ell,b}^\dagger c_{\ell+1,a} + \text{h.c.} \right), \\ H_V &= V \sum_{\ell=1}^N n_{\ell,a} n_{\ell,b} + V \sum_{\ell=1}^{N-1} n_{\ell,b} n_{\ell+1,a}, & H_u &= \sum_{\ell=1}^N \sqrt{2} e^{-i\pi/4} u (n_{\ell,a} - n_{\ell,b}). \end{aligned} \quad (30)$$

At first glance, it appears that large V favors double degenerate manifolds, represented by

$$|\text{CDW-1}\rangle = |0_{1,a} 1_{1,b} \cdots 0_{N,a} 1_{N,b}\rangle \quad \text{and} \quad |\text{CDW-2}\rangle = |1_{1,a} 0_{1,b} \cdots 1_{N,a} 0_{N,b}\rangle, \quad (31)$$

where all N fermions are on either b sublattices for CDW-1 or a sublattices for CDW-2, and they contribute zero repulsion potential energy $e_0 = 0$. When CDW-2 on the left side of the chain adjoins CDW-1 on the right side of the chain, a kink “ $0_{\ell,b} 0_{\ell+1,a}$ ” is formed at the junction between the ℓ -th and $(\ell + 1)$ -th unit cells without costing any repulsion potential energy. The corresponding state is represented by the basis $|s_\ell\rangle = |\cdots 1_{\ell,a} 0_{\ell,b} 0_{\ell+1,a} 1_{\ell+1,b} \cdots\rangle$. Specifically, $|s_0\rangle = |\text{CDW-1}\rangle$ for $\ell = 0$, while $|s_N\rangle = |\text{CDW-2}\rangle$ for $\ell = N$.

We define a projector as $P = \sum_{\ell=0}^N |s_\ell\rangle \langle s_\ell|$, which represents a part of the Hilbert space. Additionally, we have the projector $Q = \mathbb{1} - P$ representing the rest of the Hilbert space. By taking into account the perturbative part H_1 , we can obtain an effective Hamiltonian, i.e.,

$$H_{\text{eff}} = e_0 \mathbb{1} + P H_1 P + P H_1 Q (e_0 - Q H_0 Q)^{-1} Q H_1 P = H_{\text{HN}} + H_{\text{IMP}} + H_{\text{LCP}}, \quad (32)$$

up to second-order perturbation [12, 13], where $H_{\text{HN}} = H_{\text{HN}}^{\text{NN}} + H_{\text{HN}}^{\text{NNN}}$,

$$\begin{aligned} H_{\text{HN}}^{\text{NN}} &= \sum_{\ell=0}^{N-1} (t_R |s_\ell\rangle \langle s_{\ell+1}| + t_L |s_{\ell+1}\rangle \langle s_\ell|), & H_{\text{HN}}^{\text{NNN}} &= -\frac{1}{V} \sum_{\ell=0}^{N-2} (t_R^2 |s_\ell\rangle \langle s_{\ell+2}| + t_L^2 |s_{\ell+2}\rangle \langle s_\ell|), \\ H_{\text{IMP}} &= -\frac{t_1^2 + t_2^2 - \gamma^2}{V} (|s_0\rangle \langle s_0| + |s_N\rangle \langle s_N|) + \text{const.}, & H_{\text{LCP}} &= \sum_{\ell=0}^N \sqrt{2} e^{-i\pi/4} u (2\ell - N) |s_\ell\rangle \langle s_\ell|. \end{aligned} \quad (33)$$

The Hamiltonian H_{HN} describes the generalized Hatono-Nelson (HN) model, which includes hoppings $H_{\text{HN}}^{\text{NN}}$ between the nearest-neighboring (NN) indices as well as $H_{\text{HN}}^{\text{NNN}}$ between the next-nearest-neighboring (NNN) indices, with direction-dependent hopping amplitudes. Due to the broken t_2 -bond between two edges of the chain, in the Hamiltonian H_{IMP} , the real chemical potential strength for the bases $|s_0\rangle$ and $|s_N\rangle$ is lower than that of the other bases. This effectively introduces impurities (IMP) for $\ell = 0$ and N . Lastly, the staggered chemical potential defined in the main text becomes a linear chemical potential (LCP) $\mu_{\text{eff}} = u(1 - i)(2\ell - N)$ in the Hamiltonian H_{LCP} , which varies linearly with the location of the kink.

B. Non-Hermitian charge density wave

When $t_1 > \gamma$ and $u = 0$, under a generalized gauge transformation defined by operators $\eta = \bar{\eta}^{-1} = \prod_{\ell=1}^N \exp[g(\ell - 1)n_{\ell,a} + g\ell n_{\ell,b}]$, the pseudo-Hermitian Hamiltonian H in Eq. (30) can be converted into a Hermitian counterpart $H^{(\text{h})} = \bar{\eta} H \eta = H_{\tilde{t}_1} + H_{t_2} + H_V$, where

$$H_{\tilde{t}_1} = \tilde{t}_1 \sum_{\ell=1}^N (c_{\ell,a}^\dagger c_{\ell,b} + \text{h.c.}). \quad (34)$$

Furthermore, one has $t_{L/R} = t_1 \mp \gamma = \tilde{t}_1 \exp(\mp g)$. By finding an eigenstate $|\Psi^{(h)}\rangle$ for the Hamiltonian $H^{(h)}$, we can obtain the eigenstates of the non-Hermitian one as $\langle \bar{\Psi} | = \langle \Psi^{(h)} | \bar{\eta}$ and $|\Psi\rangle = \eta |\Psi^{(h)}\rangle$.

The Hermitian Hamiltonian (34) exhibits inversion symmetry, suggesting that an even-parity superposition $|\Psi^{(h)}\rangle = (|\text{CDW-1}\rangle + |\text{CDW-2}\rangle)/\sqrt{2}$ is the unique ground-state wave function for finite N . Thus the non-Hermitian counterpart is given by

$$|\Psi\rangle = \eta |\Psi^{(h)}\rangle \propto |\text{CDW-1}\rangle + e^{-gN} |\text{CDW-2}\rangle . \quad (35)$$

Due to the fact that $g > 0$, CDW-1 dominates in the right eigenstate $|\Psi\rangle$ because the ratio e^{-gN} becomes zero in the thermodynamic limit (TDL). In contrast, only CDW-2 survives in the left eigenstate $\langle \bar{\Psi} |$ in the TDL.

C. Condition for the existence of a kink

Let us consider the simple case of $u = 0$ in the \mathcal{PT} -unbroken region of the Hamiltonian (32), where $H_{\text{eff}} = H_{\text{HN}} + H_{\text{IMP}}$. In this scenario, there are two possible cases: (1) When the Hamiltonian H_{HN} is dominant, the kink is allowed to move in the chain and has a kinetic energy of $e_K = -2\tilde{t}_1$ as $N \rightarrow \infty$. (2) When H_{IMP} becomes dominant, the ground state prefers one of the manifolds $|s_0\rangle$ and $|s_N\rangle$, where the kink is eliminated by releasing the chemical potential energy of $e_P = (\tilde{t}_1^2 + t_2^2)/V > 0$. Therefore, the kink survives only if the chemical potential energy released for eliminating a kink is larger than the kinetic energy gained for adding a kink, i.e., $-e_P > e_K$ or equivalently $2V\tilde{t}_1 < \tilde{t}_1^2 + t_2^2$. This condition qualitatively defines the transition line $V_c = (\tilde{t}_1^2 + t_2^2)/(2\tilde{t}_1)$ from the nCDW phase to the nCDW_k phase in the ground-state phase diagram Fig. 2(a), as $V \rightarrow +\infty$.

D. Lowest excitation gap Δ in the nCDW_k state

When V is extremely large, we consider only the leading-order term $H_{\text{HN}}^{\text{NN}}$ in Eq. (33), which gives an energy dispersion of $\epsilon_m = 2\tilde{t}_1 \cos p_m$ and the lattice spacing is set to 1. In this case, the momentum $p_m = m\pi/(N+2)$, where the integer $m = 1, \dots, N+1$. It is important to note that $N+1$ is the number of bases considered. The ground-state energy of the nCDW_k state is given by $e_0 = \epsilon_{N+1} = -2\tilde{t}_1 \cos[\pi/(N+2)]$. For the second lowest-energy state, we get its energy $e_1 = \epsilon_N = -2\tilde{t}_1 \cos[2\pi/(N+2)]$. So the gap for the lowest excitation is given by

$$\Delta = e_1 - e_0 = \chi \left[\cos\left(\frac{\pi}{N+2}\right) - \cos\left(\frac{2\pi}{N+2}\right) \right] \quad (36)$$

with $\chi = \chi_0 = 2\tilde{t}_1$. To include the NNN hoppings $H_{\text{HN}}^{\text{NNN}}$ in Eq. (33), the energy dispersion can be approximated as $\epsilon_m \approx 2\tilde{t}_1 \cos p_m - (2\tilde{t}_1^2/V) \cos(2p_m)$ in the limit of $N \rightarrow +\infty$. As a result, the renormalized prefactor is obtained by

$$\chi = \chi_0 + \frac{4\tilde{t}_1^2}{V} \left[\cos\left(\frac{\pi}{N+2}\right) + \cos\left(\frac{2\pi}{N+2}\right) \right] \approx \chi_0 + \frac{8\tilde{t}_1^2}{V} > \chi_0 , \quad (37)$$

as N approaches infinity. When the impurity chemical potential term H_{IMP} is introduced, the prefactor χ becomes larger. For the original model (30), the scaling of the gap is given numerically by bbDMRG and shown in Fig. 2(c) of the main text, which keeps consistent very well with Eq. (36) and (37).

IV. BENCHMARKS OF OTHER NON-HERMITIAN MODELS

In Fig. 2, we provide additional benchmarks of the ground-state energy in other non-Hermitian models, including \mathcal{PT} -symmetric SSH chain of interacting fermions [14], non-Hermitian spin-1/2 XXZ chain [15], non-Hermitian Aubrey–André–Harper (AAH) Bose-Hubbard chain [16]. It is worth noting that in the ordinary \mathcal{PT} -symmetric SSH chain studies in Ref. [14], we also introduce the repulsive interaction term H_V defined in Eq. (30). These results further demonstrate the efficiency of the bbDMRG algorithm, where the absolute errors of the ground-state energy consistently converge with the truncation dimension $m = 100$ or even less, and the values approach the double-precision limit of floating-point numbers.

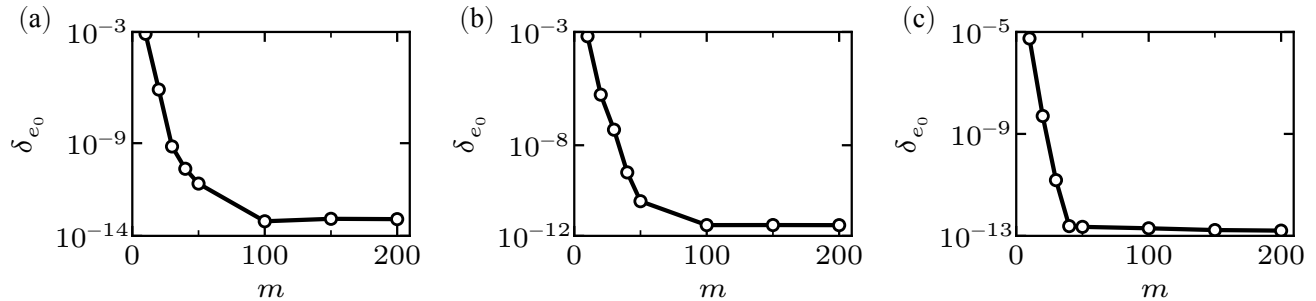


FIG. 2. Absolute errors δ_{e_0} of the ground-state energy as a function of the truncation dimension m used in bbDMRG. We consider several non-Hermitian quantum models, including (a) The \mathcal{PT} -symmetric SSH chain [14] of 24 sites with the parameters $v_1 = v_2 = \sin(\pi/8)$, $w_1 = w_2 = \cos(\pi/8)$, $u = 0.3$, and $V = 2$ at half filling. (b) The non-Hermitian spin-1/2 XXZ chain [15] of 24 sites with parameters $J = 1$ and $\Delta_\gamma = 1.5 + 0.5i$. (c) The non-Hermitian Aubrey–André–Harper (AAH) Bose-Hubbard chain [16] of 18 sites with parameters $J = V = 1$, $\gamma = 0.4$, $\alpha = 1/3$, $\delta = 2\pi/3$, and $U = 4$ at 1/3-filling. In the Fock bases for each site, the maximum number of bosons is limited to 4.

* haiqing0@csrc.ac.cn

† xiaoqunwang@zju.edu.cn

‡ shijiehu@csrc.ac.cn

- [1] U. Schollwöck, The density-matrix renormalization group in the age of matrix product states, *Annals of Physics January 2011 Special Issue*, **326**, 96 (2011).
- [2] L. Mirsky, A trace inequality of John von Neumann, *Monatshefte für Mathematik* **79**, 303 (1975).
- [3] X.-D. Zhang, *Matrix Analysis and Applications* (Cambridge University Press, 2017).
- [4] M. T. Chu, R. E. Funderlic, and R. J. Plemmons, Structured low rank approximation, *Linear Algebra and its Applications Special Issue on Structured Matrices: Analysis, Algorithms and Applications*, **366**, 157 (2003).
- [5] Z. Bai and J. W. Demmel, On swapping diagonal blocks in real schur form, *Linear Algebra and its Applications* **186**, 75 (1993).
- [6] R. E. Hartwig, Roth’s removal rule revisited, *Linear Algebra and its Applications* **49**, 91 (1983).
- [7] R. H. Bartels and G. W. Stewart, Algorithm 432 [c2]: Solution of the matrix equation $ax + xb = c$ [f4], *Communications of the ACM* **15**, 820 (1972).
- [8] L. Kohaupt, Introduction to a Gram-Schmidt-type biorthogonalization method, *Rocky Mountain Journal of Mathematics* **44**, 10.1216/RMJ-2014-44-4-1265 (2014).
- [9] J. Wilkening, An algorithm for computing Jordan chains and inverting analytic matrix functions, *Linear Algebra and its Applications* **427**, 6 (2007).
- [10] S. Hu, B. Normand, X. Wang, and L. Yu, Accurate determination of the Gaussian transition in spin-1 chains with single-ion anisotropy, *Physical Review B* **84**, 220402 (2011), publisher: American Physical Society.
- [11] A. Honecker, S. Hu, R. Peters, and J. Richter, Dynamic and thermodynamic properties of the generalized diamond chain model for azurite, *Journal of Physics: Condensed Matter* **23**, 164211 (2011).
- [12] M. Takahashi, Half-filled Hubbard model at low temperature, *Journal of Physics C: Solid State Physics* **10**, 1289 (1977).
- [13] F. Mila and K. P. Schmidt, Strong-Coupling Expansion and Effective Hamiltonians, in *Introduction to Frustrated Magnetism: Materials, Experiments, Theory*, Springer Series in Solid-State Sciences, edited by C. Lacroix, P. Mendels, and F. Mila (Springer, Berlin, Heidelberg, 2011) pp. 537–559.
- [14] S. Lieu, Topological phases in the non-Hermitian Su-Schrieffer-Heeger model, *Physical Review B* **97**, 045106 (2018).
- [15] K. Yamamoto, M. Nakagawa, M. Tezuka, M. Ueda, and N. Kawakami, Universal properties of dissipative Tomonaga-Luttinger liquids: Case study of a non-Hermitian XXZ spin chain, *Physical Review B* **105**, 205125 (2022).
- [16] D.-W. Zhang, Y.-L. Chen, G.-Q. Zhang, L.-J. Lang, Z. Li, and S.-L. Zhu, Skin superfluid, topological Mott insulators, and asymmetric dynamics in an interacting non-Hermitian Aubry-Andre-Harper model, *Physical Review B* **101**, 235150 (2020).